Molecular Biology of the Cell
Vol. 15, 4911–4925, November 2004

Echovirus 1 Endocytosis into Caveosomes Requires Lipid Rafts, Dynamin II, and Signaling Events[V]

Vilja Pietiäinen,*† Varpu Marjomäki,‡ Paula Upla,‡ Lucas Pelkmans,§‖ Ari Helenius,‖ and Timo Hyypiä*¶

*Department of Virology, Haartman Institute, University of Helsinki, FIN-00014 Helsinki, Finland; ‡Department of Biological and Environmental Science, University of Jyväskylä, FIN-40351 Jyväskylä, Finland; §Max Planck Institute for Molecular Cell Biology and Genetics, D-01307 Dresden, Germany; ‖Swiss Federal Institute of Technology Zürich (ETH), CH-8093 Zürich, Switzerland; and ¶Department of Virology and MediCity Research Laboratory, University of Turku, FIN-20520 Turku, Finland

Submitted January 29, 2004; Revised August 17, 2004; Accepted August 24, 2004
Monitoring Editor: Jean Gruenberg

Binding of echovirus 1 (EV1, a nonenveloped RNA virus) to the $\alpha 2\beta 1$ integrin on the cell surface is followed by endocytic internalization of the virus together with the receptor. Here, video-enhanced live microscopy revealed the rapid uptake of fluorescently labeled EV1 into mobile, intracellular structures, positive for green fluorescent protein-tagged caveolin-1. Partial colocalization of EV1 with SV40 (SV40) and cholera toxin, known to traffic via caveosomes, demonstrated that the vesicles were caveosomes. The initiation of EV1 infection was dependent on dynamin II, cholesterol, and protein phosphorylation events. Brefeldin A, a drug that prevents SV40 transport, blocked the EV1 infection cycle, whereas drugs that disrupt the cellular cytoskeleton had no effect. In situ hybridization revealed the localization of viral RNA with endocytosed viral capsid proteins in caveosomes before initiation of viral replication. Thus, both the internalization of EV1 to caveosomes and subsequent events differ clearly from caveolar endocytosis of SV40 because EV1 uptake is fast and independent of actin and EV1 is not sorted further to sER from caveosomes. These results shed further light on the cell entry of nonenveloped viral pathogens and illustrate the use of viruses as probes to dissect caveolin-associated endocytic pathways.

INTRODUCTION

Viruses that enter host cells by endocytosis are important tools in studies of membrane traffic in animal cells. Recently, they have been used to identify novel endocytic mechanisms that bypass the classical clathrin-mediated uptake processes (Pelkmans *et al.*, 2001; Meier *et al.*, 2002). We have previously reported echovirus 1 (EV1) to be one of the viruses entering host cells via caveolar endocytosis (Marjomäki *et al.*, 2002; Upla *et al.*, 2004); however, the cellular mechanisms involved in the process are still incompletely defined.

Echoviruses are human pathogens that can cause meningitis, encephalitis, rash, and mild respiratory and enteric infections (Grist *et al.*, 1978). Echoviruses belong to the Picornavirus family of small (30 nm), nonenveloped, positive-stranded RNA viruses. They include such significant pathogens of humans and livestock as polioviruses (PV), rhinoviruses (HRV), hepatitis A virus (HAV), and foot-and-mouth disease viruses (FMDV). In spite of their close structural relationships, a variety of entry routes into host cells, including clathrin-mediated endocytosis, caveolae, and lipid rafts, are used by different picornaviruses (DeTulleo and Kirchhausen, 1998; Joki-Korpela *et al.*, 2001; Marjomäki *et al.*, 2002; Stuart *et al.*, 2002).

EV1 recognizes the $\alpha 2$I domain of the $\alpha 2\beta 1$ integrin, a collagen receptor, on the cell surface (Bergelson *et al.*, 1994), leading to uptake of the receptor and the virus through caveolae-mediated endocytosis (Marjomäki *et al.*, 2002). Caveolae are invaginations of the plasma membrane ~50–80 nm in size (Palade, 1953), and their main protein component is caveolin-1 (Rothberg *et al.*, 1992). They are involved in various signaling processes and in uptake of cholesterol (Murata *et al.*, 1995; Simons and Toomre, 2000). The other ligands include autocrine motility factor (AMF; Benlimame *et al.*, 1998) and cholera toxin (CTX; Montesano *et al.*, 1982) as well as microbial pathogens such as type FimH-expressing *Escherichia coli* (Shin *et al.*, 2000), and SV40 (SV40; Anderson *et al.*, 1996). Even though caveolae are relatively stable under normal conditions, interaction of the ligand with a receptor can trigger their internalization in the presence of protein phosphorylation, dynamin II GTPase, and actin (Parton *et al.*, 1994; Henley *et al.*, 1998). The endocytosed caveolar vesicles accumulate in a discrete population of preexisting, caveolin-1–containing mobile structures

Article published online ahead of print. Mol. Biol. Cell 10.1091/mbc.E04–01–0070. Article and publication date are available at www.molbiolcell.org/cgi/doi/10.1091/mbc.E04–01–0070.

[V] The online version of this article contains supplementary material accessible through http://www.molbiolcell.org.

† Corresponding author. E-mail address: vilja.pietiainen@helsinki.fi.

Abbreviations used: AF, Alexa Fluor-594; BFA, brefeldin A; Bis, bisindolylmaleimide; CTX, cholera toxin; Cy5, cyan 5 dye; CytD, cytochalasin D; EV1, echovirus 1; FISH, fluorescent in situ hybridization; Gen, genistein; GFP, green fluorescent protein; HRV, human rhinovirus; Jas, jasplakinolide; LatA, latrunculin A; MBCD, methyl-β-cyclodextrin; NaOV, sodium orthovanadate (Na_3VO_4); Noco, nocodazole; Nys, nystatin; OA, okadaic acid; p.i., postinfection (indicates time after 1-h incubation of EV1 at 4°C); PFU, plaque-forming unit; Prog, progesterone; PV, poliovirus; Saf, safingol; SV40, simian virus 40; TxR, Texas Red.

called caveosomes (Pelkmans *et al.*, 2001), which take up extracellular ligands such as CTX (Nichols, 2002), AMF (Le *et al.*, 2002), and SV40 and cholesterol (Pelkmans *et al.*, 2001).

CTX is further sorted from caveosomes to the Golgi complex (Le and Nabi, 2003), SV40 (Pelkmans *et al.*, 2001), and AMF (Le and Nabi, 2003) are transported to the endoplasmic reticulum (ER), whereas the location of EV1 before initiation of replication has thus far remained unclear. Picornaviruses are known to undergo structural alterations during receptor interactions and entry, leading to the uncoating of the virus particle and release of the viral genome into the cytoplasm required for subsequent translation and replication events (Hogle, 2002). Uncoating of pH-sensitive picornaviruses, such as HRVs, takes place in the acidic pH environment of endosomes or by rupture of endosomes (Schober *et al.*, 1998; Huber *et al.*, 2001). However, because EV1 is acid-pH-stable, it must rely on other mechanisms and possibly other organelles for entry and uncoating.

Here, the uptake mechanism of EV1 was further studied using a fluorescently labeled virus and GFP-constructs of caveolin-1 in a real-time live microscopy, dominant negative mutants of cellular proteins, and different inhibitors of cellular functions. We show that after binding to the $\alpha 2\beta 1$ integrin EV1 is rapidly endocytosed into caveosomes, a process dependent on dynamin II, cholesterol, and protein phosphorylation events but not requiring an intact actin cytoskeleton or microtubules. The viral capsid proteins and RNA are found in the caveosomes until the initiation of viral replication. The EV1 entry process provides a new model for studies on endocytosis of microbial pathogens and caveosome function.

MATERIALS AND METHODS

Cell Culture, Virus Purification, and Fluorescent Labeling

EV1 (Farouk strain) was obtained from the American Type Culture Collection (ATCC, Manassas, VA). The virus was grown in a green monkey kidney (GMK; ATCC) cell line and purified in sucrose gradients (Pietiäinen *et al.*, 2000). The fluorescent labeling of purified EV1, with a 10 times higher molar concentration of Texas Red-X succinimidyl ester (Molecular Probes, Eugene, OR) and Alexa Fluor (AF)-594 succinimidyl ester (Molecular Probes), was performed as described by Pelkmans *et al.* (2001). The infectivity of the labeled virus (AF-EV1) was determined by plaque titration, and the efficiency of labeling was calculated from the absorbance spectrum. To reveal the labeled proteins, a sample of AF-EV1 was run in a 12% SDS-PAGE gel that was stained with a silver staining kit (Amersham Pharmacia Biotech, Piscataway, NJ) after UV exposure. SV40 was propagated in a green monkey kidney cell line (CV-1; ATCC), purified and labeled with Cy5, FITC, or AF-594 dyes as reported (Pelkmans *et al.*, 2001).

Most of the experiments were performed in the CV-1 cell line (green monkey kidney cell line; ATCC), which was maintained as described earlier (Pelkmans *et al.*, 2001). The SAOS-$\alpha 2\beta 1$ cell line was generated from SAOS cells (ATCC), which do not normally express the $\alpha 2$ integrin subunit (Ivaska *et al.*, 1999). Infections of the cells with EV1 and SV40 were performed in appropriate cell culture media supplemented with 1% FCS. Multiplicity of infection (MOI) of 2 or 20 was used in EV1 infections. The EV1 infections were performed for 1 h at 4°C to allow the binding of the virus before removal of the unbound virus by washing and transferring the cells to 37°C.

Antibodies and Immunofluorescence Microscopy

The following primary antibodies were used in the immunofluorescent staining: rabbit anti-EV1 antibody (Marjomäki *et al.*, 2002) to detect EV1 capsid proteins, rabbit anticaveolin-1 antibody (N-20; Santa Cruz Biotechnology, Santa Cruz, CA), mouse monoclonal anticaveolin-1 antibody (2234; Transduction Laboratories, Lexington, KY), anti-CD49b mAb recognizing the I domain of the $\alpha 2$ integrin subunit (Immunotech, Marseille, France), AF-488-labeled (Molecular Probes) mouse anti-$\alpha 2$ mAb (MCA2025, Serotec, Oxford, United Kingdom), mouse anti-p230 mAb for detecting the trans-Golgi network (Transduction Laboratories), mouse mAb against PDI (ID3; from S. Fuller, University of Oxford, Oxford, United Kingdom), rabbit antitransferrin antibody (Behring Institute, Marburg, Germany), goat antibody against syntaxin 17 (Steegmaier *et al.*, 1998), rabbit antiserum against cation-independent-mannose-6-phosphate receptor (CI-MPR; Marjomäki *et al.*, 1990), and mouse mAb for CD63 (Zymed, South San Francisco, CA).

AF-488–conjugated cholera toxin subunit B (0.5 or 10 μg/ml; Molecular Probes) was incubated with CV-1 cells together with EV1 for 1 h at 4°C, and the cells were then transferred to 37°C. Lysotracker Red DND99 (100 nM; Molecular Probes) was added to EV1-infected cells for 30 min at 37°C. Holo-transferrin (Sigma, St Louis, MO) was incubated with cells in the growth medium at a concentration of 1 mg/ml for 10 min at 37°C. AF-594–labeled SV40 (10^3 PFU/cell) was added to the cells for 2 h at 37°C before EV1 binding to cells in cold. For nocodazole assay, CV-1 and SAOS-$\alpha 2\beta 1$ cells were treated with nocodazole (33 μM) for 30 min at 37°C and incubated with Cy5-SV40 (1 $\mu g/10^5$ cells) for 1.5 h at 37°C before addition of EV1 at 37°C. Depolymerization of microtubules was verified by tubulin labeling. After incubation at 37°C for an appropriate time, the cells were fixed with 4% formaldehyde (Sigma), quenched with 50 mM NH_4Cl, and permeabilized with 0.05% (wt/vol) saponin (Sigma) or 0.3% Triton X-100 (Sigma) in PBS.

AF-488– and -568–conjugated anti-mouse, anti-goat, and anti-rabbit secondary antibodies (Molecular Probes) were used to recognize the primary antibodies, and mouse anti-HA antibody (BabCO, Richmond, CA) to recognize the HA-tag. The cells were mounted with a mounting medium containing 90% glycerol and 1% *n*-propyl-gallate (Sigma) and examined either with an axiovert confocal microscope (Leica TCS SP2, Wetzler, Germany) with an HCX PL APO 63×/1.32–0.6 oil objective or with Axiovert 100 M SP epifluorescence microscope (Carl Zeiss, Jena, Germany) equipped with a confocal setup (Zeiss LSM510), using a Plan Neofluar objective (63×/1.25 oil). Sequential scan for different laser lines was used to avoid a false colocalization signal. Images obtained with Leica confocal microscope were collected with a cooled charge-coupled-device (CCD) camera and processed using the Leica confocal software program (LCS-Lite). Images obtained with Zeiss confocal microscope were processed using LSM program (Carl Zeiss). All the figures were converted to TIFF format for further processing and editing in Photoshop (Adobe, San Jose, CA) and FreeHand 8 (Macromedia, San Francisco, CA). For quantification of infection percentages of stained samples, images were taken with an Olympus BX50 immunofluorescence microscope containing a CCD camera (Hamamatsu, Shizuoka, Japan), using a U Plan FI 20×/0.5 Ph1 objective and the Open Lab 2.2.5 program (Improvision, Lexington, MA). At least four sections containing ~300 cells were counted for each specimen.

Transfections

The transient transfections of CV-1 cells were performed for 14 h before EV1 infection with FuGENE 6 (Roche, Basel, Switzerland) or Superfect (Qiagen, Chatsworth, CA) following manufacturers' protocols. N- or C-terminally GFP-tagged constructs of caveolin-1 (GFP-caveolin-1 and caveolin-1-GFP, respectively; Pelkmans *et al.*, 2001) were used in (real-time) microscopy and infectivity measurements. HA-tagged caveolin-3 and caveolin-3^{DGV} (Roy *et al.*, 1999) were obtained from Robert Parton (University of Queensland, Brisbane, Australia), GFP-dynamin 2aa and GFP-dynamin $2aa^{K44A}$ (Cao *et al.*, 1998; Ochoa *et al.*, 2000) from Mark McNiven (Mayo Clinic, Rochester, MN), Eps15-GFP and Eps15EΔ 95/295-GFP (Benmerah *et al.*, 1999) from Alice Dautry-Varsat (Institute Pasteur, Paris, France), and adaptor protein 180 mutant (AP180C construct; Ford *et al.*, 2001) from Dieter Blaas (University of Vienna, Austria). The EV1 infection was allowed to proceed in transfected cells for 6 h at 37°C before immunostaining or collection the samples for the plaque assay.

Time-lapse Fluorescence Microscopy

AF-EV1 was bound to untransfected or GFP-tagged caveolin-1–transfected CV-1 cells for 1 h at 4°C. FITC-labeled SV40 (10^3 PFU per cell) was incubated with untransfected cells for 90 min at 37°C, before binding of AF-EV1 for 1 h at 4°C. Microscopy was performed at 37°C using a Zeiss Axiovert wide-field microscope with a 100× NA 1.4 plan-apochromat lens, a computer-controlled shutter, and standard FITC/Alexa Fluor-594 filters. Images were collected with a CCD camera, with 2× binning, delay times of 4–10 s, and exposure times of 0.5–1 s/image. In addition, the delay of 330 ms between FITC/AF-594 filters was recorded. The collected images were further processed using Open Lab 2.2.5 software and edited to QuickTime 5 format. The color for AF-EV1 was set as red (except as white in video corresponding to Figure 2D), and the color for SV40 and GFP constructs as green, before merging of images, which resulted in a yellow color when colocalization occurred. For calculating movements and velocities, the location of the object was marked in several frames, which were then merged to measure the distance traveled between frames. To quantitate colocalization, Pearson's coefficient was calculated using the Open Lab program.

Drug Treatments

CV-1 cells were incubated with different drugs for 30 min at 37°C before addition of EV1 for 1 h at 4°C, which was followed by a 6-h incubation period at 37°C. Concentrations of the drugs were 5 μM bisindolylmaleimide (Sigma), 5 μg/ml cytochalasin D (Sigma), 25–250 μM genistein (Sigma), 1 μM latrunculin A (Molecular Probes), 0.5 μM jasplakinolide (Molecular Probes), 10 mM methyl-β-cyclodextrin (Sigma), 33 μM nocodazole (Sigma), 25 μg/ml nystatin (Sigma) together with 10 μg/ml progesterone (Sigma), 1 μM okadaic acid (Sigma), 10 μM safingol (Sigma), and 1 mM sodium orthovanadate (Calbio-

chem, La Jolla, CA). Immunofluorescent staining and plaque titration (Marjomäki *et al.*, 2002) were performed for collected samples.

For dose-dependent assay with drugs affecting the actin cytoskeleton, poly-L-lysine coating of the coverslips was performed to prevent the deattachment and rounding of the cells. Poly-L-lysine, 1 μg/ml, in PBS was added on coverslips in the previous day and washed away before plating of the CV-1 cells. Actin drugs (cytochalasin D; 1–7 μg/ml, latrunculin A; 0.13–1 μM and jasplakinolide; 0.1–0.75 μM) were added to the cells for 30 min at 37°C before EV1 infection and immunofluorescent staining assay performed as described above.

For testing the effects of brefeldin A (BFA, Sigma), the CV-1 cells were incubated in the presence of the drug (0.5–2 μg/ml) for 1 h at 37°C. EV1 infection and detection of infected cells were performed as above. To investigate the time-scale of its action, BFA was added to cells at different time points of infection (−1, 0, 1, 2, 3, and 4 h). The infections were allowed to proceed for 6 h at 37°C before the plaque assay and/or immunofluorescent staining of infected cells. To study the effect of BFA on the intracellular localization of EV1, BFA was added 1 h before infection or 1 h postinfection (p.i.). To investigate whether SV40 is localized into the same cellular structures with EV1, BFA was added 1 h p.i. to the cells infected with Cy5-SV40 and EV1 as described earlier in *Materials and Methods*, and the infections were let to proceed until 3–4 h before fixation and immunofluorescent staining.

Infection Titration and Immunoblotting

CV-1 cells, infected with EV1 (MOI 20), were collected at different time points and after three freeze-thaw cycles, the amount of virus was determined by quantitative plaque analysis (Marjomäki *et al.*, 2002). For Western blot analysis, infected cells were collected at appropriate time points, boiled in 2× SDS-lysis buffer, and electrophoresed in a 12% SDS-PAGE gel. The immunoblotted proteins were reacted with anti-EV1 antibody and detected using horseradish-peroxidase (HRP)-conjugated swine anti-rabbit IgG (DakoCytomation, Glostrup, Denmark). Signals were detected using an enhanced chemiluminescence Western blotting detection kit (Amersham Pharmacia Biotech).

Sucrose Gradient Sedimentation Analysis

Metabolic labeling of purified EV1 and PV1 was performed using ^{35}S-methionine (50 μCi/ml; Amersham Pharmacia Biotech; Marjomäki *et al.*, 2002). To prepare 135S and 80S control particles for the gradients, ^{35}S-labeled PV1 was incubated with GMK cells for 15 min at 37°C, and the supernatant containing the unbound virus was collected. To prepare the EV1 samples, 20,000 cpm of the ^{35}S-labeled virus was incubated with GMK cells for 1 h at 4°C to allow binding of the virus before incubation period of 1–2 h at 37°C. Preparation of the samples and ultracentrifugation in linear 5–20% sucrose gradients were performed as detailed elsewhere (Marjomäki *et al.*, 2002).

Fluorescent In Situ Hybridization

The full-length cDNA clone of EV1 in the pSPORT 1 vector (Ohman *et al.*, 2001) was provided by Jeffrey Bergelson (Children's Hospital of Philadelphia, Philadelphia, PA). The negative-polarity RNA strand was transcribed using SP6 polymerase (Promega, Madison, WI) from linearized EV1 cDNA in the presence of FITC-labeled UTP (0.35 mM; Molecular Probes) or Chromatide Alexa Fluor-546–14-UTP (0.175 mM; Molecular Probes). After DNase I treatment, the probe was purified as described earlier (Bolten *et al.*, 1998). To perform fluorescent in situ hybridization (FISH), the untransfected and GFP-caveolin-1–transfected CV-1 cells were infected with EV1, and the hybridization reaction was performed for 12 h at 42°C in the dark, in the presence of the labeled probe (Bolten *et al.*, 1998). After removal of the unbound probe, the cells were mounted with 2.5% DABCO (Sigma) in pH-buffered glycerol and visualized using a confocal microscope (Leica) as described above.

RESULTS

EV1 Is Endocytosed into CV-1 Cells That Express the Viral Receptor

Most of the experiments in this study were performed in CV-1 cells, a green monkey kidney cell line in which the caveolar pathway of SV40 has been characterized (Pelkmans *et al.*, 2001, 2002). As shown in Figure 1A (1st row), the surface of uninfected CV-1 cells stained weakly positive for the EV1 receptor, α2β1 integrin, which did not colocalize with caveolin-1. In contrast, EV1 infection of the cells triggered internalization of the integrin molecules partially into caveolin-1–containing organelles, as judged by confocal images obtained from the focal plane in the center of the cell (Figure 1A, 2nd row; 2 h at 37°C). Staining with anti-EV1 antibody illustrated that some of these organelles also contained EV1 (Figure 1A, 3rd row). Thus, the virus interacted with the CV-1 cells in a similar manner as with SAOS-α2β1 cells, which we have used in previous studies of EV1 internalization (Marjomäki *et al.*, 2002; Upla *et al.*, 2004).

EV1 caused rapid and efficient infection of the CV-1 cells, and production of infectious progeny virus particles was observed at 4 h p.i. (Figure 1B). Six hours after infection most of the cells (~75%) showed cytopathic effect and stained intensively with an antibody against EV1 (our unpublished results). Immunoblotting using antibodies against the EV1 capsid proteins revealed synthesis of structural proteins starting ~4 h after the infection (Figure 1C).

Properties of Fluorescently Labeled EV1

To follow the entry process by real-time fluorescence microscopy, EV1 was labeled with the amino-reactive, fluorescent dyes Texas Red (TxR) and Alexa Fluor-594 (AF). The label was bound to outer capsid proteins VP1 and VP2/VP3 of a virus particle (Figure 2A), and based on absorbance spectra, each viral particle carried 500–900 dye molecules. Labeling did not have a significant effect on the infectivity of the virus, because in the plaque titration assay the titer of AF-EV1 was at least 85% of that of unlabelled virus. When fluorescently labeled EV1 was incubated with cells at 4°C, small dots and some larger spots were observed on the cells, probably representing single viral particles and virus clusters, respectively (Figure 2B).

To investigate whether the fluorescently labeled EV1 was able to enter cells similarly to the unlabelled virus, we first used the SAOS-α2β1 cells, used in our previous studies (Marjomäki *et al.*, 2002). The cells, which were incubated for 2 h at 37°C with fluorescently labeled EV1, exhibited colocalization of the virus with α2β1 integrin and caveolin-1 in confocal microscopy (Figure 2C). Evidently, the labeled virus behaved similarly to the native virus with respect to colocalization with caveolin-1 and α2β1 integrin in SAOS-α2β1 cells.

Echovirus 1 Rapidly Moves to Caveolin-1–containing Structures after Binding to the Cell Surface

To synchronize the uptake process, we incubated CV-1 cells with AF-EV1 for 1 h at 4°C before transfer to 37°C in a preheated chamber of a real-time microscope. Some of the small dots on the cell surface could now be seen to join larger spots of different sizes. Although most of these spots remained stationary, some moved out of the focal plane, suggesting endocytic uptake (Figure 2D; Supplementary Video Figure 2D_v). When the experiment was repeated in GFP-tagged caveolin-1–expressing CV-1 cells, the majority of virus particles bound to the cells at 4°C did not colocalize with caveolin-1 on the cell surface. However, after 10 min at 37°C, viruses moved into caveolin-1–positive mobile structures in the cell periphery and deeper in the cytoplasm. These structures were likely to be intracellular based on their mobility and their location (Figure 2E; Supplementary Video Figure 2E_v).

Kinetics of EV1 Traffic in the Cells

Within the first 20 min at 37°C, the viruses became increasingly associated with larger, caveolin-1–positive structures (Figure 3, A and B). By focusing, it became clear that the viruses were located in intracellular organelles. During an 8–22-min incubation at 37°C the colocalization analysis of caveolin-1 and EV1 in live microscopy images revealed an increase of ~75% in Pearson's correlation, a figure related to the extent of overlap between the images (Manders *et al.*, 1993). Although some of these virus-containing organelles were stationary, the majority were

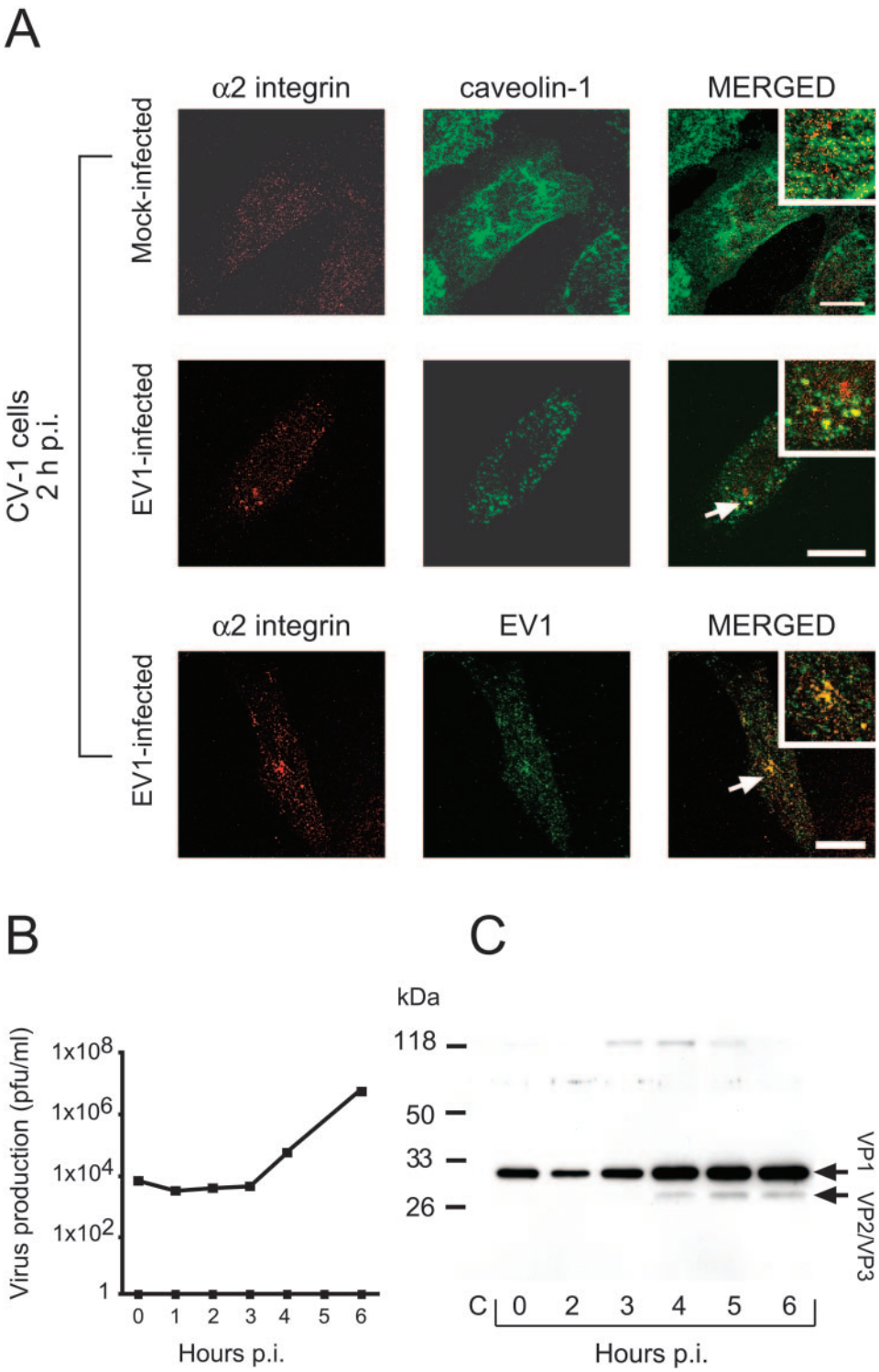

Figure 1. Expression of $\alpha 2\beta 1$ integrin and caveolin-1, and synthesis of the infectious virus in CV-1 cells. (A) Mock-infected CV-1 cells, immunostained for cell-surface $\alpha 2$ integrin (red) and for caveolin-1 (green), expressed molecules on the cell surface (first row). In EV1-infected cells, the integrin (red) showed partial intracellular colocalization with caveolin-1 (green; second row) and EV1 (green; third row) at 2 h p.i. Bars, 20 μm. (B) Infectious EV1 particles were produced in CV-1 cells after 3 h p.i., as determined using the plaque titration assay. (C) The amount of EV1 capsid proteins (VP1, VP2/VP3, indicated by arrows) increased in the cells at 4 h p.i., when analyzed using anti-EV1 antibody in immunoblot analysis. The most immunoreactive VP1 band, seen in the first three lanes (0, 2, and 3 h p.i.), represents the inoculated virus particles.

mobile. They typically performed random, short-distance movements of 3–6 μm or medium-distance movements of 9–14 μm (Figure 3, A-I; Supplementary Videos Figures 3A_v1 and 3A_v2). The velocities of their motion varied from 0.02–0.3 μm/s. Some vesicles carried out directional long-distance movements of 20–38 μm at irregular intervals, with a speed of 0.04–0.15 μm/s (Figure 3A-II; Supplementary Video Figure 3A_v3).

At 90 min or later, caveolin-1–GFP-negative, tubular structures (length 5 μm) containing AF-EV1 were sometimes observed (2 h p.i.; Figure 3A-III; Supplementary Video Figure 3A_v4). In addition, thin structures (length 4–11 μm) containing caveolin-1 but no virus could occasionally be distinguished (Figure 3B; Supplementary Video Figure 3B_v). EV1-containing caveosomes were seen to move along these structures (Figure 3B; Supplementary Video Figure 3B_v).

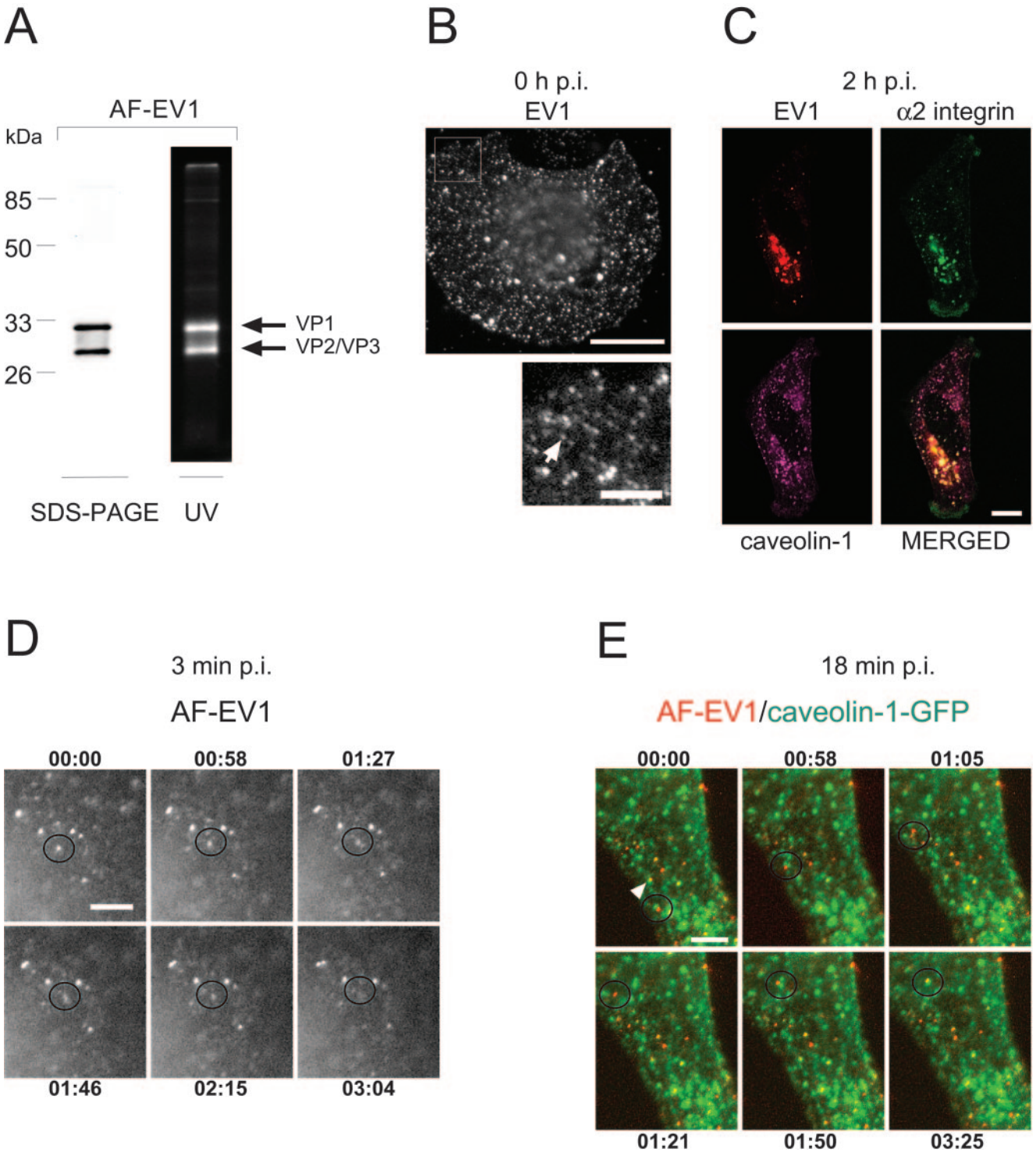

Figure 2. Characterization of fluorescently labeled EV1 and its uptake into the cell. (A) SDS-PAGE analysis of AF-594-labeled EV1 by silver staining (left) and by UV exposure (right) indicates that the major capsid proteins were fluorescently labeled. (B) Fluorescent virus spots, present on the CV-1 cell surface after incubation of the cells with AF-EV1 (8×10^4 EV1 particles/cell) for 1 h at 4°C (top). A detail of a picture presenting the viral particles (see arrow) is shown below. Bars, 20 and 5 μm, respectively. (C) Fluorescently labeled EV1 colocalizes with $\alpha 2\beta 1$ integrin and caveolin-1. The labeled virus (red) and the AF-488-labeled antibody against $\alpha 2$ integrin (green) were incubated with SAOS-$\alpha 2\beta 1$ cells for 2 h at 37°C, and the fixed cells were stained for caveolin-1 (purple). Colocalization is shown in the merged image. Bar, 10 μm. (D) AF-EV1 entry into CV-1 cells at 3 min p.i. The fluorescently labeled virus was bound to the cells for 1 h at 4°C followed by incubation at 37°C under a real-time microscope. The figures illustrate accumulations of viral particles on the cell surface and their entry into the cell (Supplementary Video Figure 2D_v). The time elapsed from the beginning of recording (3 min p.i.) is noted in each frame. Bar, 5 μm. (E) Association of AF-EV1 with caveolin-1–containing structures at 18 min p.i. In AF-EV1–infected (red), caveolin-1-GFP (green)–transfected CV-1 cells, virus particles (indicated by a circle) were observed to associate with caveolin-1–containing structures (Supplementary Video Figure 2E_v). In addition, some viral particles were already associated with caveolin-1–containing structures at the beginning of the observation period (indicated by an arrow). The time elapsed from the beginning of recording (18 min p.i.) is noted in each frame. Bar, 5 μm.

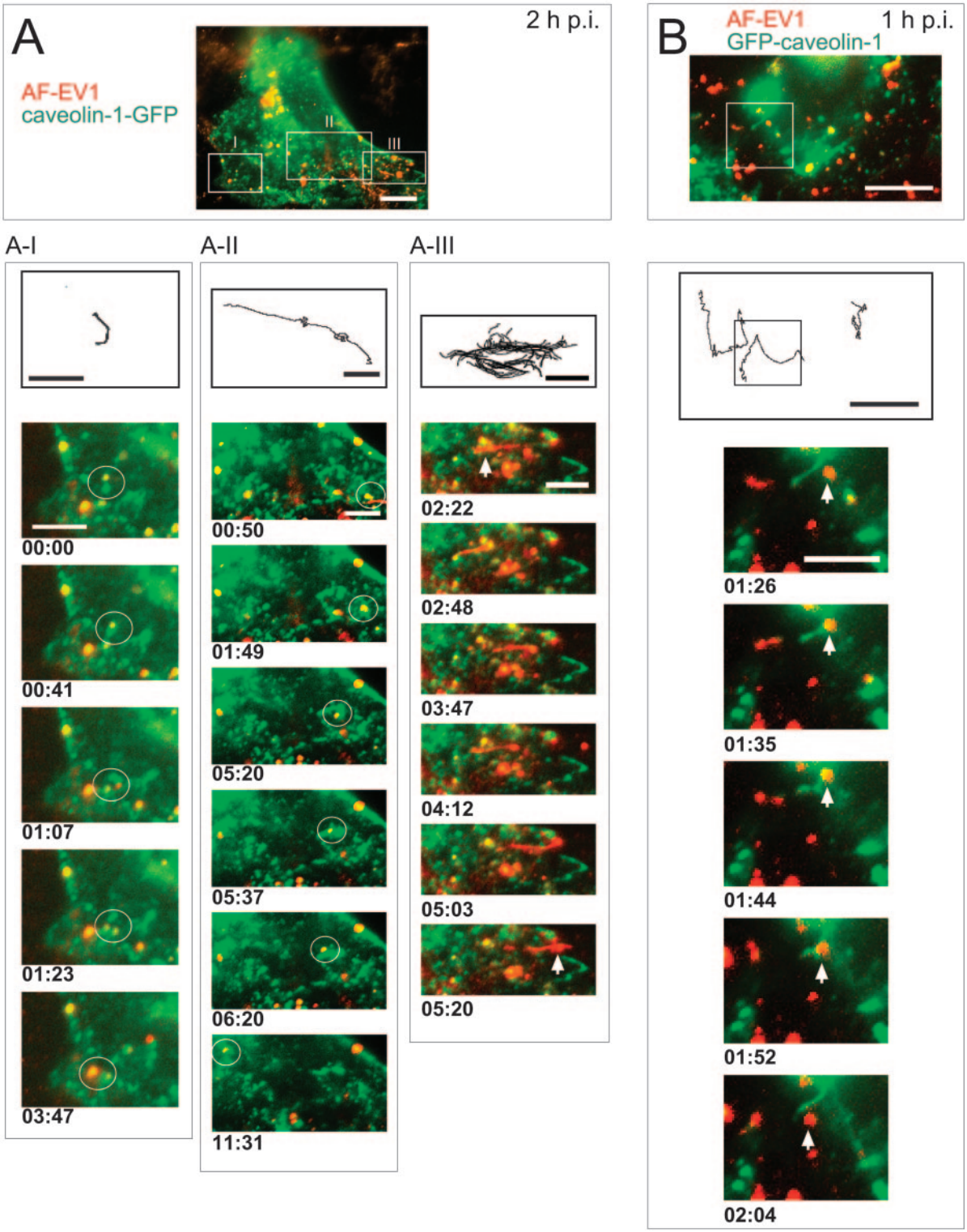

Figure 3. Viral traffic in caveolar vesicles in living CV-1 cells. AF-EV1 (red) was bound to GFP-tagged caveolin-1 (green)–transfected CV-1 cells for 1 h at 4°C and then transferred to 37°C under a real-time fluorescence microscope. Colocalization is shown in yellow in the merged images. The routes of vesicles are shown in black lines above the recordings. The time elapsed from the beginning of recording is noted under each frame. The boxed areas are shown in the insets. Bars, 10 μm (whole cell) and 5 μm (frames). (A) Different types of movements of EV1-positive caveosomal vesicles in the caveolin-1-GFP–expressing cells at 2 h p.i. Caveosomal vesicles carrying the virus particles showed random short-distance movements (white circle; A–I; Supplementary Videos Figures 3A_v1 and 3A_v2), whereas some of the vesicles exhibited rapid long-distance movements along curvilinear paths in the cytoplasm (A-II; Supplementary Video Figure 3A_v3). EV1 was occasionally transported along tubular-like formations from caveolar vesicles to the cell boundaries (A-III; Supplementary Video Figure 3A_v4). (B) Different types of movements in GFP-caveolin-1–expressing cells at 1 h p.i. Caveolin-1–containing tubular structures were involved in virus transport (Supplementary Video Figure 3B_v).

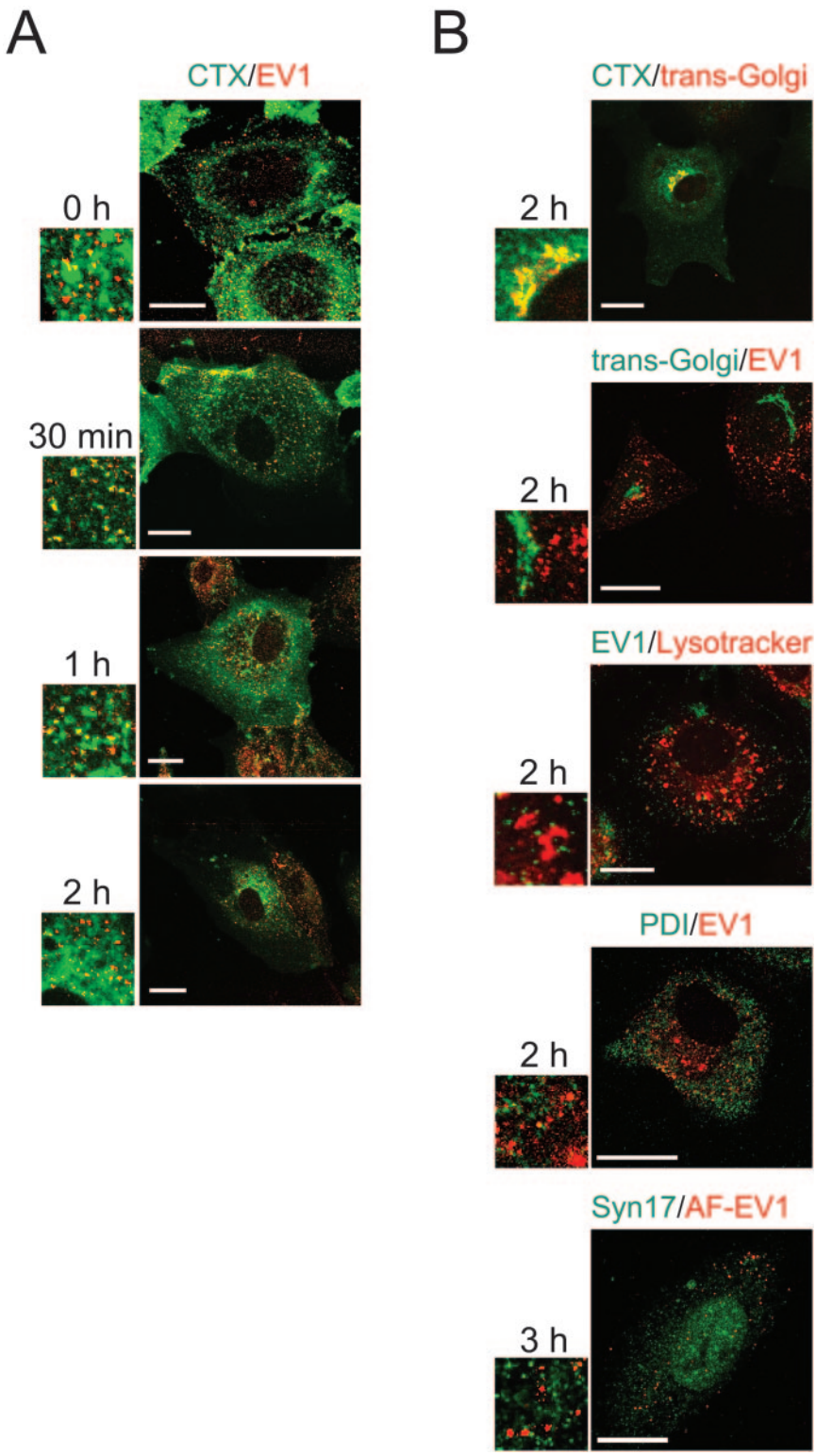

Figure 4. Localization of EV1, CTX and different cellular markers in CV-1 cells. (A) Intracellular colocalization of EV1 and CTX. AF-488–labeled CTX (green) was allowed to bind to cells simultaneously with EV1 (red; immunostained) for 1 h at 4°C, and the cells were transferred to 37°C. Some colocalization in confocal microscopy was observed at 30 min to 1 h p.i. in intracellular vesicles. After 1 h p.i., the colocalization diminished. Bars, 20 μm. (B) Most of the CTX (green) had reached the Golgi apparatus (red; p230 antibody against the trans-Golgi network) at 2 h p.i. (row 1). EV1 (rows 2 and 4: immunostained red; row 3: immunostained, green; row 5: AF-EV1, red) did not colocalize with trans-Golgi marker p230 (green; row 2), lysosomal marker Lysotracker (red; row 3), PDI, a rough ER marker (green; row 4), or syntaxin17, a smooth ER marker (green; row 5). Bars, 20 μm except 10 μm, row 5.

Colocalization of EV1 with CTX and SV40

Next, we determined whether the EV1-containing organelles would accumulate CTX, a ligand known to bind to a GM1 ganglioside and at least partially pass through caveosomes during transport to the Golgi complex (Nichols, 2002). When incubated on the CV1 cells together for 1 h at 4°C, followed by incubation at 37°C, CTX and AF-EV1 were found to partially colocalize in small, dot-like structures at 30–60 min (Figure 4A). After 1 h, most of the CTX had accumulated in the perinuclear region, colocalizing with trans-Golgi as detected by a specific p230 antibody (2 h p.i.; Figure 4B). Colocalization of EV1 with CTX was not observed within this region (Figure 4, A and B). Nor did EV1 colocalize with marker for lysosomes (Lysotracker) at 2 h p.i., the rough ER

(protein disulphide isomerase; PDI) at 2 h p.i. or smooth ER (syntaxin 17) at 3 h (Figure 4B) or 4 h p.i (our unpublished results). Syntaxin 17 was also stained in AF-EV1–infected SAOS-$\alpha 2\beta 1$ cells without a notable colocalization with the virus (our unpublished results).

To further characterize the EV1-containing, caveolin-1–positive organelles, CV-1 cells were incubated simultaneously with EV1 and SV40. SV40 is known to remain on the plasma membrane caveolae for at least 20 min before endocytosis via caveolar vesicles to caveosomes in 40 min to 3 h (Anderson *et al.,* 1998; Pelkmans *et al.,* 2001). To synchronize the entry processes of the more rapidly internalized EV1 and SV40, SV40 was preincubated with cells for 90 min to 2 h at 37°C before inoculation of EV1 for 1 h at 4°C. The cells were then transferred back to 37°C to allow the infections to proceed. The localization of AF-SV40 (red) and EV1 (detected by immunofluorescence, green) was studied in fixed CV-1 cells by confocal microscopy (Figure 5A). Although the viruses did not colocalize at the beginning of infection, partial colocalization was observed at 30 min after EV1 entry, and this increased during the next 2 h (Figure 5A). In live microscopy, cytoplasmic structures containing FITC-labeled SV40 and AF-EV1 were observed 15 min after EV1 entry, and these increased in size with incubation time (Figure 5B; Supplementary Video Figure 5B_v1). The SV40- and EV1-positive structures also became more mobile ~1 h after EV1 entry (Supplementary Video Figure 5B_v2). This occurred somewhat later than in cells infected with EV1 alone, suggesting that SV40 coinfection may retard the entry process. Furthermore, the CV-1 cells and SAOS-$\alpha 2\beta 1$ cells were treated for 30 min at 37°C with nocodazole (33 μM), a microtubule-disrupting agent that does not affect the SV40 uptake to caveosomes but prevents its sorting from caveosomes to sER (Pelkmans *et al.,* 2001). The nocodazole-treated cells were infected with Cy5-SV40 for 90 min at 37°C before addition of EV1, and after incubation for 2–4 h at 37°C, the cells were fixed and immunostained with antibodies against EV1. The presence of nocodazole increased the colocalization of EV1 and SV40 in both cell lines (Figure 5C), strongly supporting that the structures EV1 entered were caveosomes.

As a conclusion, the presence of caveolin-1, CTX, and SV40 in same intracellular organelles with EV1 demonstrated that EV1 entered caveosomes. The fast internalization of EV1 to caveosomes was similar to CTX but diverse from a slow uptake of SV40. The subsequent pathways are remarkably different, because SV40 is known to traffic to sER (Pelkmans *et al.,* 2001; Norkin *et al.,* 2002) and CTX was further sorted to the Golgi complex, but EV1 did not reach the Golgi or the (s)ER.

Dynamin II Is Involved in EV1 Infection

Expression of mutant constructs of caveolin-1, caveolin-3, dynamin II, Eps15, and AP180 was next used to analyze the cellular requirements for EV1 infection. Hemagglutin (HA)-tagged, truncated and dominant-negative caveolin-3 (cav-3^{DGV}; lacking the first 53 amino acids) disrupts lipid transport and causes depletion of lipid rafts, thus inhibiting caveolar endocytosis (Parton *et al.,* 1997; Roy *et al.,* 1999). Cav-3^{DGV} showed 35% inhibition of EV1 infection (Figure 6A). Cav-3^{DGV} is known to inhibit SV40 infection in a very similar manner by ~30% (Roy *et al.,* 1999). In contrast to cav-3^{DGV}, N-terminally GFP-tagged caveolin-1 (GFP-caveolin-1; Pelkmans *et al.,* 2001) has an overall distribution with similar to that of wild-type caveolin-1, and it has been used in live microscopy studies of caveolar function (Thomsen *et al.,* 2002). Here, the outcome of GFP-caveolin-1 in EV1 infection was tested because it serves as a dominant negative inhibitor of SV40 entry (Pelkmans *et al.,* 2001). In contrast to its effect on SV40, GFP-caveolin-1 did not affect the uptake (see Figures 3B and 9) and replication of EV1 (our unpublished results).

Dynamin II is a widely needed GTPase that acts both in clathrin-coated pit and caveolar internalization (Damke *et al.,* 1994; Henley *et al.,* 1998; Oh *et al.,* 1998). We found that the expression of the dominant-negative mutant of dynamin II, dyn2(K44A), inhibited EV1 infection by 75% in CV-1 cells (Figure 6A). In contrast, the dominant-negative deletion mutant of Eps15, Eps15(EΔ95/295), which prevents formation of clathrin-coated vesicles (Benmerah *et al.,* 1999), did not inhibit EV1 infection (Figure 6A). The Eps15(EΔ95/295) construct was functional because it inhibited transferrin endocytosis in the CV-1 cells (our unpublished data). In addition, a mutant of adaptor protein 180 (AP180C), that interferes clathrin route (Ford *et al.,* 2001; Snyers *et al.,* 2003), was tested, and like Eps15, it had no significant effect because it inhibited the EV1 infection only by ~7%. In addition, studies with dominant negative mutants of Eps15 and AP180 in SAOS-$\alpha 2\beta 1$ cells strongly suggest that the clathrin-mediated pathway is not involved in the antibody-induced internalization of the viral receptor, $\alpha 2\beta 1$ integrin (Upla *et al.,* 2004). These results demonstrate the requirements for dynamin II as well as caveolin but not clathrin in the initiation of EV1 infection.

Role of Cholesterol, Signaling Events, and Cellular Cytoskeleton in EV1 Infection

The effects of several inhibitors on EV1 infection were examined using immunofluorescence and the plaque titration assay (Figure 6B). The cells were pretreated with the drugs for 30 min at 37°C, and the drugs remained present during the entire infection period. First, to find whether cholesterol and lipid rafts play a role in EV1 infection, the combination of progesterone (Prog; a cholesterol synthesis inhibitor, 10 μg/ml) and nystatin (Nys; a cholesterol-sequestering drug, 25 μg/ml; Simons and Toomre, 2000) was tested, showing inhibition by more than 50%. Further evidence for involvement of lipid rafts and/or caveolae was seen in treatment with 10 mM methyl-β-cyclodextrin (MBCD), which affects cholesterol distribution and destroys caveolae (Hailstones *et al.,* 1998), inhibiting EV1 infection almost completely (by 95%).

Internalization of caveolae depends on specific signaling events (Simons and Toomre, 2000), including activation of protein kinase C (Mineo *et al.,* 1998) and local tyrosine phosphorylation (Nomura and Fujimoto, 1999; Pelkmans *et al.,* 2002). Here, we tested the effects of a broad-spectrum protein kinase C (PKC) inhibitor, bisindolylmaleimide (Bis; 5 μM), and a specific PKCα inhibitor, safingol (Saf; 10 μM). Both inhibitors prevented infection efficiently (≥80%), demonstrating the involvement of PKCα in the process (Figure 6B), as has also been observed in EV1 infection in SAOS-$\alpha 2\beta 1$ cells (Upla *et al.,* 2004). Moreover, genistein (Gen), a specific tyrosine kinase inhibitor, was able to block infection in a dose-dependent manner when studied by the immunofluorescence assay (proportion of infected cells in the presence of genistein: 250 μM, 0%; 100 μM, 13%; 50 μM, 28%; 25 μM, 86%; no genistein, 100%; Figure 6B; 100 μM). Okadaic acid (OA; 1 μM), a general inhibitor of serine and threonine phosphatases that has been reported to increase caveolar internalization (Parton *et al.,* 1994) did not have a significant effect. Unexpectedly, the treatment with sodium orthovanadate (NaOV; 1 mM), an inhibitor of protein ty-

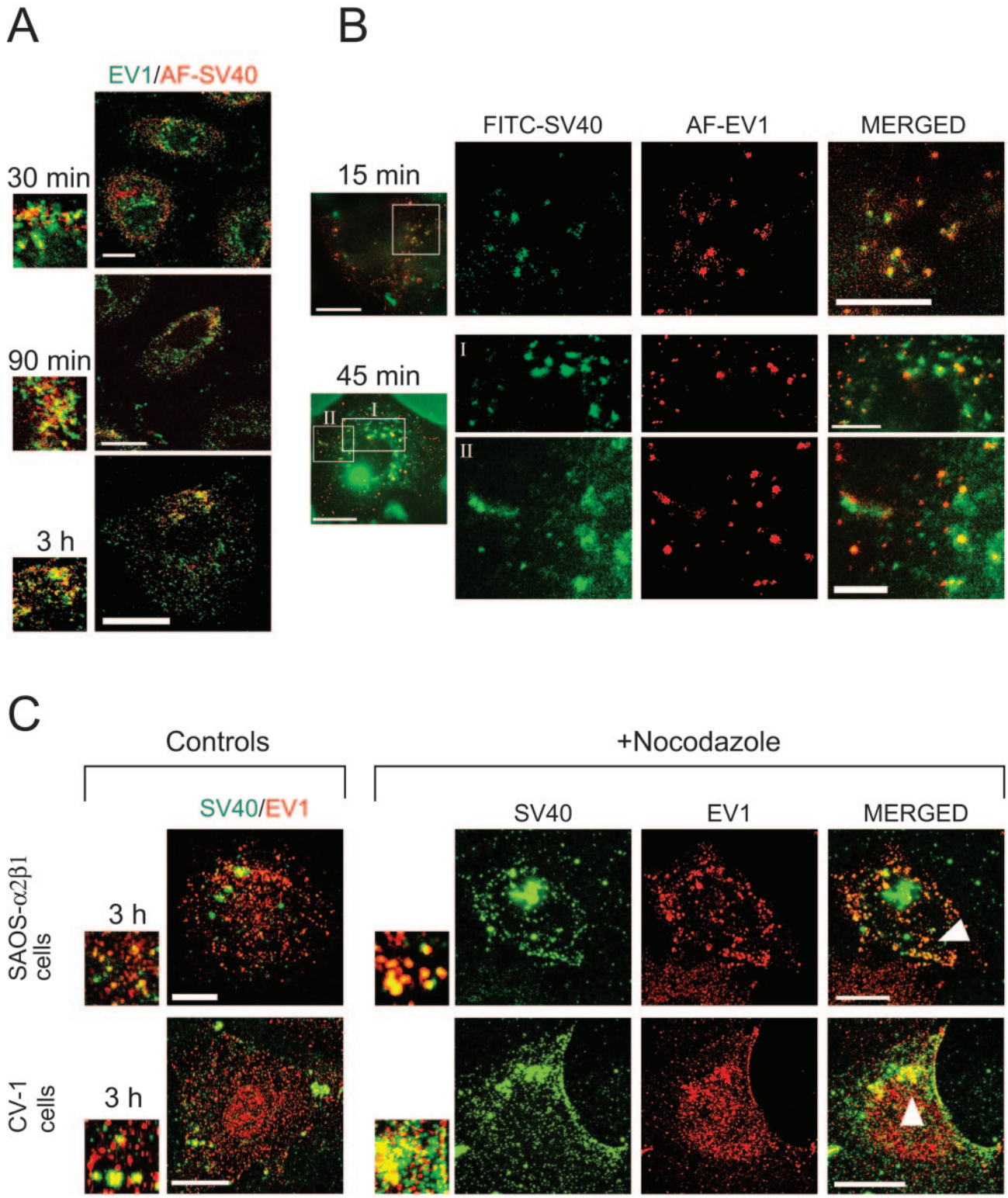

Figure 5. Colocalization of EV1 and SV40 in CV-1 and SAOS-$\alpha 2\beta 1$ cells. (A) Colocalization of EV1 (recognized with anti-EV1 antibody; green) with AF-SV40 (red) in confocal microscopy of coinfected CV-1 cells. Colocalization was observed in smaller structures and in perinuclear accumulations in merged confocal images. Bars, 20 μm. (B) Colocalization of AF-EV1 (red) and FITC-SV40 (green) in wide-field real-time microscopy of coinfected CV-1 cells. Still images at 15 and 45 min p.i. show a partial colocalization of SV40 and EV1 in caveosome-like structures (Supplementary Videos Figures 5B_v1 and 5B_v2). Bars, 20 μm (whole cell), 10 μm (1st and 2nd rows), and 5 μm (3rd row). (C) The CV-1 and SAOS-$\alpha 2\beta 1$ cells were pretreated with a microtubule-disrupting agent nocodazole (33 μM) that prevents SV40 traffic from caveosomes but does not affect EV1 infection and then coinfected with Cy5-SV40 and EV1. The increase in EV1 (immunostained as red) and Cy5-SV40 (Cy5 processed as green) colocalization was observed in the drug-treated SAOS-$\alpha 2\beta 1$ cells (row 1) and CV-1 cells (row 2) at 3 h p.i. Bars, 10 μm, row 1 and 20 μm, row 2.

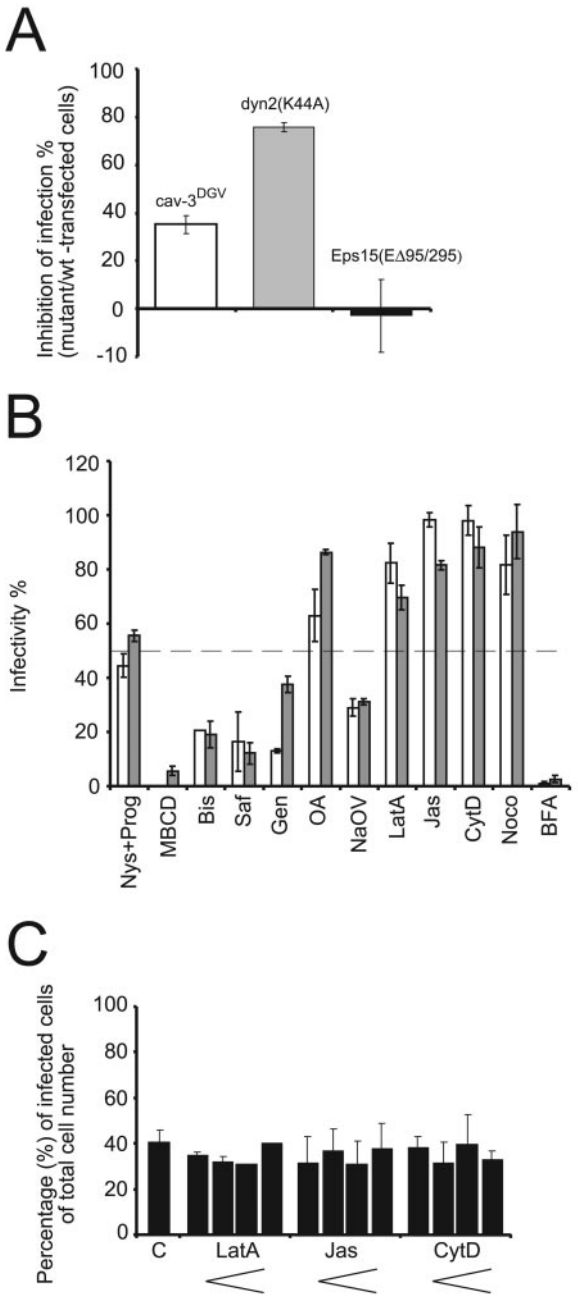

Figure 6. The effects of dominant negative mutant constructs of cellular proteins and different inhibitors of cellular processes on EV1 infection. (A) EV1 infection was impeded in cells expressing the mutant forms of caveolin-3 (cav-3^{DGV}) and dynamin II [dyn2(K44A)], but the Eps15 mutant [Eps15(EΔ95/295)] had no effect on infectivity at 6 h p.i. The mean infection percentages of mutant construct-transfected cells were compared with wild-type construct–transfected cells (±SE). (B) The inhibitors of cellular cholesterol balance and signaling events impeded EV1 infection. CV-1 cells were pretreated with different inhibitors before 6-h infection with EV1. Abbreviations and concentrations of the drugs are described in *Results.* The mean infectivity percentages from the immunofluorescent staining assay (white columns; ± SE), and from the plaque titration assay (gray columns; ± SD) are presented. (C) The actin-disturbing agents CytD, LatA, and Jas showed no dose-response effect on EV1 infection in CV-1 cells. Concentrations used for LatA were 0.13, 0.33, 0.66, and 1 μM, for Jas 0.1, 0.25, 0.5, and 0.75 μM and for CytD 1, 2.5, 5, and 7.5 μg/ml. The mean infectivity percentages (±SD) in the absence and presence of the drugs are presented.

rosine phosphatases that enhances the uptake of SV40 through caveolae (Pelkmans *et al.*, 2002), reduced EV1 infection by 70% (Figure 6B).

As actin is known to mediate the internalization of the ligands from cell surface caveolae (Parton *et al.*, 1994; Pelkmans *et al.*, 2002), we examined three agents interfering with actin function, latrunculin A (LatA, an actin monomer–sequestering drug, 1 μM), jasplakinolide (Jas, an actin polymer–stabilizing drug, 0.5 μM), and cytochalasin D (CytD, an inhibitor of actin polymerization, 5 μg/ml) (Figure 6B). A dose-dependent titration assay with these drugs showed no effect on EV1 infection in CV-1 cells (Figure 6). Nocodazole, (Noco, 33 μM), a microtubule-disrupting agent, which prevents the transport of SV40 from caveosomes to the smooth ER (Pelkmans *et al.*, 2001) had no inhibitory effect on EV1 infection (Figure 6B), even though tubular structures containing the virus have been observed in our live microscopy studies (Figure 3, A and B).

We also carried out the series of experiments with BFA, which is an inhibitor of caveolae-mediated endocytosis and a Golgi-disrupting agent (Dinter and Berger, 1998; Richards *et al.*, 2002). BFA prevented the EV1 infection completely even at low concentrations (0.5–2 μg/ml; Figure 6B; 2 μg/ml). In an assay testing which stage of infectious cycle is affected by BFA, the drug (0.5 μg/ml) exhibited more effective inhibition when added to EV1-infected CV-1 cells before 3 h p.i (Figure 7A). By confocal microscopy we observed that EV1 was able to enter the cells in the presence of BFA, but the virus was found in large accumulations (Figure 7B). To further characterize these structures, the cells were pretreated with BFA before the infection and labeled with antibodies against caveolin-1, an endosomal pathway marker (CI-MPR) and a lysosomal marker (CD63). The organelles were positive for caveolin-1 but showed no staining for CI-MPR and CD63 (our unpublished results). Also, the localization of Cy5-SV40 and EV1 was examined in presence of BFA (added 1 h p.i) in CV-1 cells (Figure 7B) and SAOS-$\alpha 2\beta 1$ cells (our unpublished results). In both cell lines, the BFA treatment caused EV1 to accumulate to greater extent into the large structures mentioned above that labeled strongly positive for both SV40 and caveolin-1 (Figure 7B). Moreover, in the presence of BFA, newly synthesized viral RNA could not be detected in cells with fluorescent in situ hybridization even at 5 h p.i. (our unpublished results), when viral RNA was observed throughout the cytoplasm in EV1-infected, untreated control cells (see Figure 8C).

From these results, we concluded that initiation of EV1 infection requires cholesterol as well as signaling events. Actin or microtubules did not appear to play a significant role in the initiation of EV1 infection. BFA, an agent blocking SV40 entry and infection (Norkin *et al.*, 2002), caused accumulation of EV1 into caveosome-like organelles and prevented the productive infection.

Colocalization of EV1 Capsid Proteins, Viral RNA, and Caveolin-1 during Virus Entry

To follow disassembly of incoming virus particles, ^{35}S-methionine–labeled EV1 was allowed to interact with GMK cells, another green monkey kidney cell line, previously used in our studies (Xing *et al.*, 2004). Sucrose gradient sedimentation of cell surface-bound EV1 showed that binding did not trigger changes in the sedimentation of the virus because the majority of virus particles (85%) were in the 160S form, representing intact viral particles (Figure 8A). Polioviral (PV1) 135S and 80S particles were produced here as controls of a well-characterized picornavirus disassembly process (Hogle 2002; Figure 8A). When EV1 was incubated

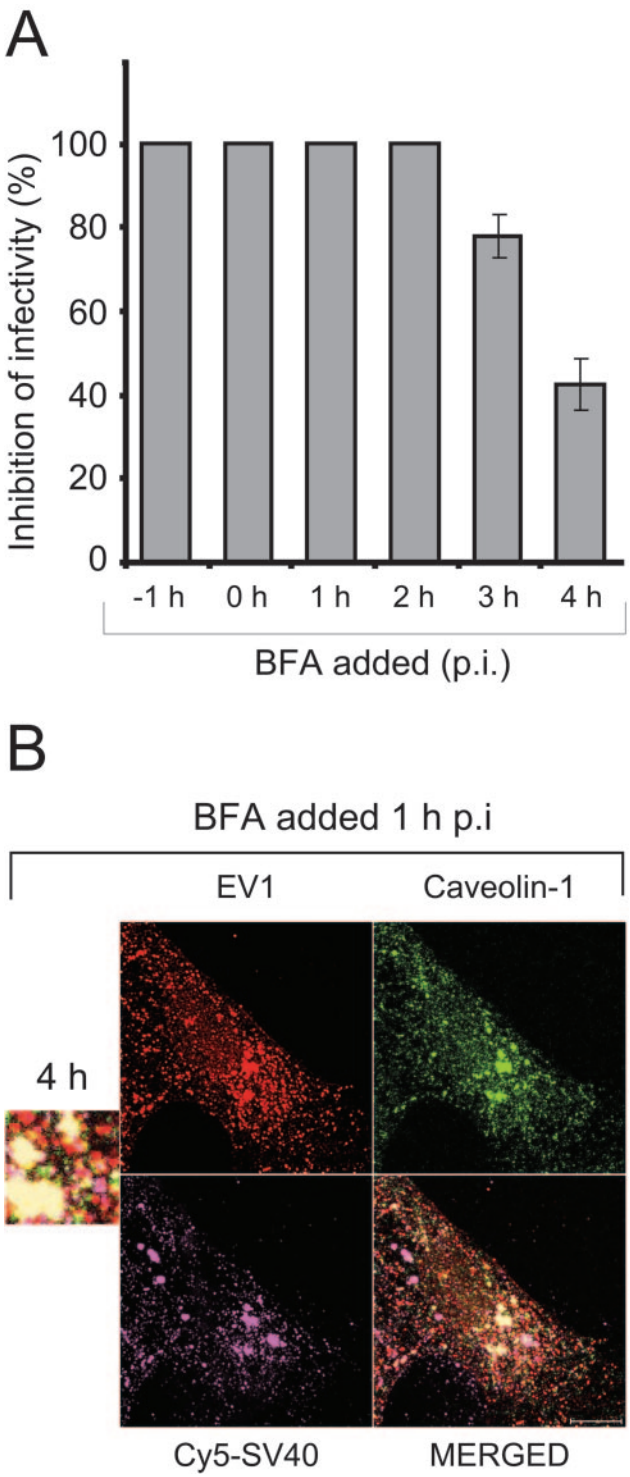

Figure 7. The effects of BFA on EV1 infection in CV-1 cells. (A) BFA was added to CV-1 cells at different time points before and after EV1 infection, the infection was let to proceed for 6 h and the inhibition of infectivity (%) was determined by immunofluorescent staining assay. BFA showed less inhibitory effect when added after 3 h p.i. The mean inhibition percentages (± SE) are presented. (B) Localization of EV1 (immunostained, red), caveolin-1 (immunostained, green) and Cy5-SV40 (purple) in CV-1 cells treated with BFA at 1 h p.i. The merged confocal figure reveals the colocalization of viruses in accumulations of caveolin-1–positive organelles in the presence of BFA. Bar, 10 μm.

with cells at 37°C for 1 h (Figure 8B), 35% of the particles were converted to the 135S form (lacking the VP4 capsid protein) and 20% to the 80S form (empty capsids without VP4 and viral genomic RNA). After 2 h of incubation at 37°C (Figure 8B), 30% of particles were in the 135S form and 30% in the 80S form. These data demonstrated that EV1 uncoating is a slow event compared with polioviruses (Hogle, 2002), and it is likely initiated after the virus has been internalized.

FISH (Bolten *et al.,* 1998) with a negative-stranded RNA probe was used to detect the viral RNA genome in CV-1 cells (Figure 8C). Genomic RNA could be observed by confocal microscopy immediately after binding of the virus as small dots on the cell surface. Already after 15 min at 37°C, the viral RNA began to concentrate into larger intracellular accumulations throughout the cytoplasm (our unpublished results). The size of the accumulations increased after 30 min, and they were also observed in the perinuclear region 1 h p.i. (Figure 8C), whereas at 2–3 h p.i. some viral RNA could also be seen along the cell boundaries. A dramatic increase in the amount of viral RNA staining was observed in the cytoplasm at 4 h p.i. (Figure 8C), consistent with the time of initiation of viral RNA replication (our unpublished results). Mock-infected control cells showed no background staining (Figure 8C).

The FISH technique was also used in combination with the detection of the fluorescent virus (AF-EV1) to follow the localization of viral RNA relative to the capsid proteins. Their colocalization could be convincingly observed 30–60 min after incubation of the infected cells at 37°C (Figure 9A). After 2 h p.i., the colocalization clearly diminished, possibly because of release of viral RNA from the virus capsids. To investigate whether the viral RNA-positive structures were caveosomes, in situ hybridization was carried out in EV1-infected, GFP-caveolin-1–transfected cells. Soon after incubation at 37°C, viral RNA was observed in small dots, without apparent colocalization with caveolin-1 (unpublished data). Colocalization of viral RNA and caveolin-1 became more evident when the infection proceeded (30 min and 1 h p.i.; Figure 9B) and when the size of the structures containing the RNA further increased (2–3 h p.i.; Figure 9B). In cells overexpressing GFP-tagged caveolin-1, the colocalization persisted even longer, possibly implying that overexpression of caveolin-1 delays the initiation of viral replication (our unpublished results). At 4 h p.i., colocalization decreased, coinciding with the onset of viral RNA synthesis (our unpublished results).

DISCUSSION

We showed that a human pathogen, EV1, enters host cells through a pathway dependent on caveosomes, dynamin II, and signaling events but not requiring clathrin-coated pits, actin filaments, or microtubules in the cell line used for the studies. Interestingly, EV1 uptake into caveosomes was much faster than that of SV40, a well-known virus model for caveolar endocytosis (Anderson *et al.,* 1996; Pelkmans *et al.,* 2001, 2002). EV1 was not observed to enter the Golgi complex, the ER, or the lysosomes, instead remaining in caveosomes until the initiation of replication. This raises a question whether caveosomes, besides sorting of viruses and other ligands to the ER or the Golgi complex, could also act as a site for virus penetration and uncoating.

Our previous study (Marjomäki *et al.,* 2002) showed that in SAOS-$\alpha 2\beta 1$ cells, overexpressing the $\alpha 2\beta 1$ integrin, the EV1 receptor, the virus entered caveolin-1–positive intracellular accumulations together with the receptor (Marjomäki

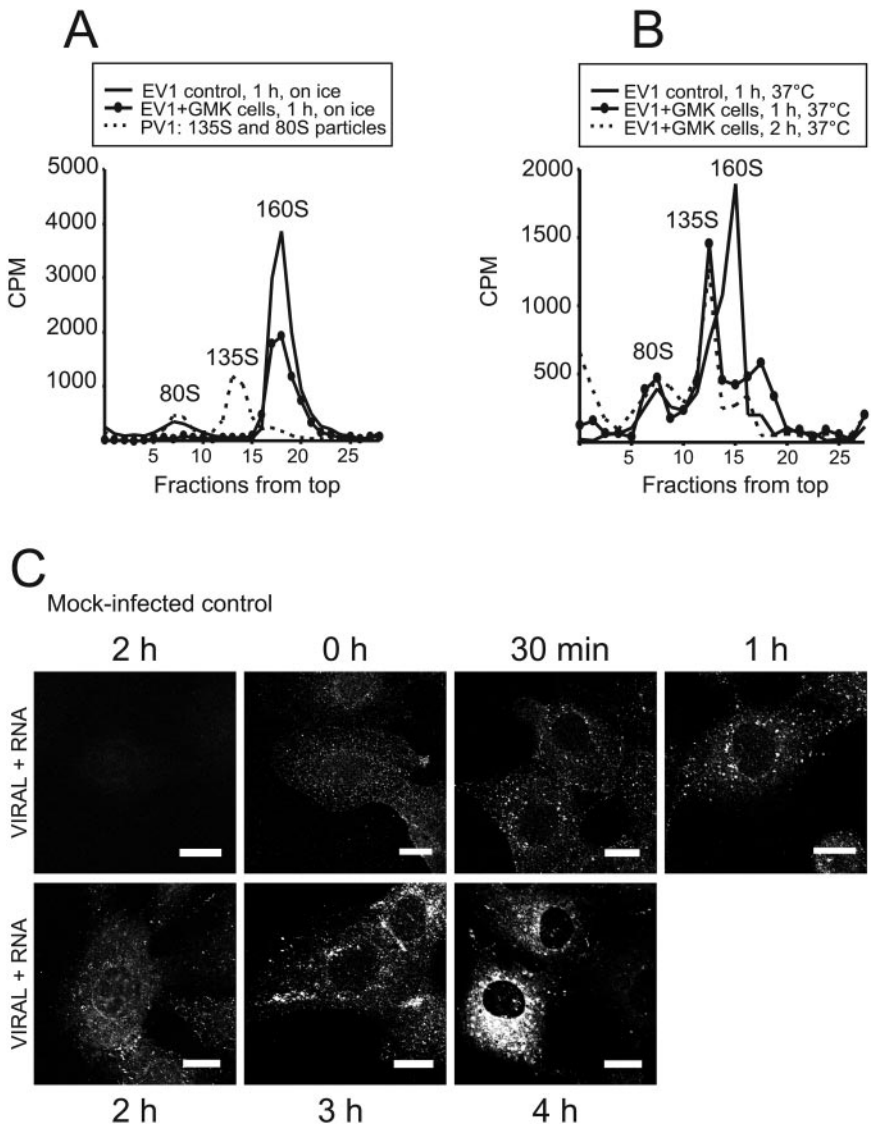

Figure 8. Conformational changes of EV1 during the entry process and the synthesis of viral RNA in infected cells. (A) Binding of ^{35}S-labeled EV1 to the GMK cells for 1 h on ice (line with circles) did not induce uncoating of the virus. Untreated EV1 remained mainly in 160S form, representing an intact capsid (solid line). PV1 markers show the sedimentation of the 135S particles lacking VP4 capsid protein and empty 80S particles. (B) After 1 h (line with circles) or 2 h (dotted line) incubation at 37°C, some viral particles had released the RNA genome, representing the 80S form, whereas the majority of the viruses still contained the RNA (135S and 160S forms). The untreated control virus had partly undergone spontaneous uncoating at 37°C. (C) The genomic viral RNA in infected CV-1 cells was detected using the FISH technique. The amount of intracellular RNA increased markedly at 4 h p.i., indicating synthesis of new viral RNA. Mock-infected control cells (2 h p.i.) did not exhibit any signal. Bars, 20 μm.

et al., 2002). Caveolar endocytosis requires dynamin (Henley *et al.*, 1998) and is a clathrin-independent process. However, dynamin II is not a specific marker of caveolar pathway because it is also needed for certain lipid raft-mediated endocytosis (Pelkmans and Helenius, 2003) and for pinching of clathrin-coated vesicles (Damke *et al.*, 1994). The experiment with dominant negative mutants of cellular proteins revealed that the infection was highly dependent on dynamin II, but was unaffected by the Eps15 mutant (Benmerah *et al.*, 1999) and the C-terminal mutant of AP180 (Ford *et al.*, 2001; Snyers *et al.*, 2003), both known to interfere the clathrin route. Accordingly, our earlier results showed that EV1 does not colocalize with transferrin, endosomal markers (Marjomäki *et al.*, 2002) or lysosomes during entry. The requirement of dynamin may exclude the recently described dynamin-independent pathways (Sabharanjak *et al.*, 2002; Pelkmans and Helenius, 2003) in EV1 uptake. The caveolar endocytosis of EV1 was further verified by inhibition of the infection with drugs interfering with the cellular cholesterol balance, with lipid rafts and with caveolae, by colocalization of the virus together with $\alpha 2\beta 1$ integrin in caveolin-1–positive intracellular structures in (live) fluorescence microscopy and by partial loss of viral infectivity (35%) in presence of a dominant-negative mutant of caveolin-3. Similar inhibition was obtained in a study where the effect of caveolin-3^{DGV} was tested on SV40 infection in CV-1 cells (Roy *et al.*, 1999). In contrast, N-terminally GFP-tagged caveolin-1, known to prevent caveolar entry of SV40 and progression of infection (Pelkmans *et al.*, 2001), did not alter EV1 uptake or infection. This suggests that either 1) the molecular interactions initiating the entry process of EV1 via cell surface caveolae might differ remarkably from SV40 or 2) parallel, noncaveolar entry mechanisms may also exist. Such an alternative pathway would need to be dynamin- and lipid raft–dependent, and result in virus transfer into caveosomes. Whether the alternative pathway is constantly functional or whether the virus is able to perform a pathway switching when cell surface caveolae are inhibited remains to be investigated.

The inhibitor experiments with genistein and PKC inhibitors revealed that tyrosine kinase–regulated phosphorylation events and activity of PKCα, enriched in caveolae (Mineo *et al.*, 1998), are involved in EV1 infection. PKCα and ERK activation has also been shown to play a role in EV1 uptake in the studies with another cell line, SAOS-$\alpha 2\beta 1$ cells (Upla *et al.*, 2004). The results are in agreement with previous findings indicating that the local protein phosphoryla-

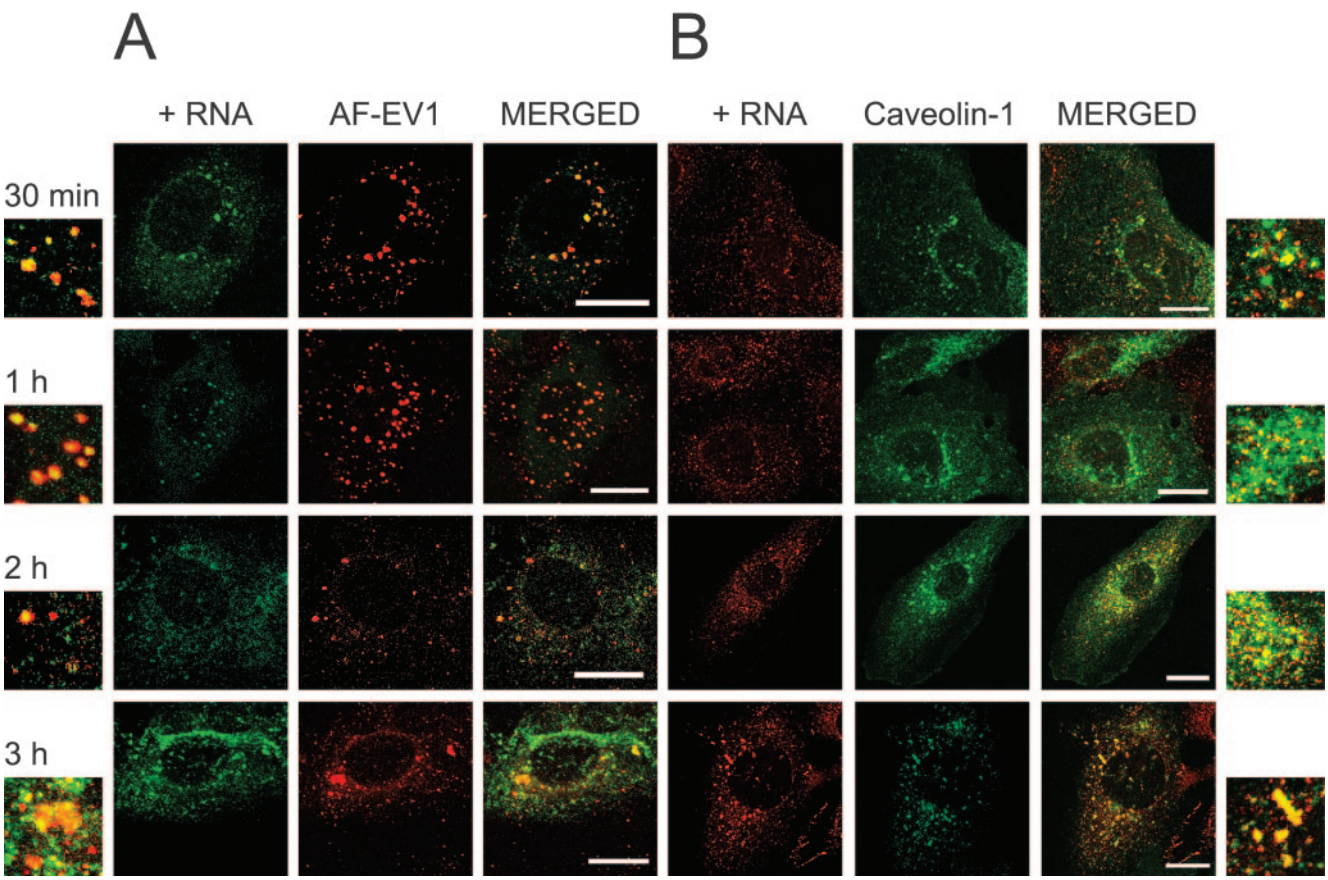

Figure 9. Colocalization of EV1 capsid proteins and viral RNA in caveosomes during endocytosis. (A) A fluorescent probe recognizing positive-stranded viral RNA was used to detect the RNA (green) in cells infected with AF-EV1 (red) using the FISH technique. Colocalization increased at 30 min p.i., as shown in the confocal images. Bars, 20 μm. (B) FISH analysis confirmed that viral RNA localized in caveosomes from 30 min p.i. to 3 h p.i. GFP-caveolin-1 (green)–transfected CV-1 cells were infected with EV1, and localization of viral RNA (red) was detected using the FISH technique. Bars, 20 μm.

tion cascade in caveolae can be induced by microbial pathogens (Pelkmans *et al.*, 2002; Sukumaran *et al.*, 2002). However, in contradiction to previous findings, showing that phosphatase inhibitors may enhance SV40 uptake through caveolae (Pelkmans *et al.*, 2002), sodium orthovanadate, a protein tyrosine phosphatase inhibitor, reduced the infectivity of EV1. Here, the drug may inhibit the alternative pathway of the EV1 entry or it may affect the infection cycle after the initial entry step of the virus.

Although internalization of SV40 in caveolae requires depolymerization of cortical actin, leading to formation of actin tails in CV-1 cells (Pelkmans *et al.*, 2002), our experiments with a concentration series of actin-disturbing agents suggested that actin was a nonessential factor in EV1 infection in CV-1 cells. Cytochalasin D treatment has recently been described to prevent the antibody-induced movement of $\alpha2\beta1$ integrin from lipid rafts to caveolae in SAOS-$\alpha2\beta1$ cells, but in agreement with our results in CV-1 cells, it did not inhibit $\alpha2\beta1$ integrin–mediated EV1 entry and infection (Upla *et al.*, 2004). These somewhat unexpected results favor the possibility that after its attachment to $\alpha2\beta1$ integrin, located in the lipid rafts on the cell surface, EV1 could enter caveolin-1–positive intracellular organelles from the lipid rafts by an actin-independent manner. This would also explain why the virus is relatively infrequently found in cell surface caveolae in electron microscopy (our unpublished results). However, one of these drugs, jasplakinolide that stabilizes actin polymers, caused a partial inhibition of EV1 infection in SAOS-$\alpha2\beta1$ cells by retaining the virus and the integrin on the cell membrane (our unpublished results), suggesting that the detailed mechanisms of EV1 uptake from the cell surface to caveosomes may vary depending on the cell type.

The real-time fluorescence microscopy of AF-EV1 entry into GFP-caveolin-1–expressing cells demonstrated an increase in colocalization of the virus and caveolin-1 ~10 min after incubation at 37°C. The structures were mainly intracellular, thus most likely being caveolin-1–containing vesicles or caveosomes. The size and number of vesicles increased over time and they became more dynamic, as described earlier for caveosomes (Pelkmans *et al.*, 2001), with speeds up to 0.3 μm/s. Trafficking led to the formation of larger accumulations, both at the cell periphery and in perinuclear regions. That the organelles were caveosomes was further confirmed by our finding that EV1 colocalized partially with CTX and SV40, which are known to be transported via caveosomes (Pelkmans *et al.*, 2001; Nichols, 2002). Moreover, nocodazole treatment that prevents the traffic of SV40 to smooth ER (Pelkmans *et al.*, 2001), increased the amount of colocalization of SV40 and EV1 in caveosomes. SV40 accumulates in caveosomes from 40 min to 3 h p.i. (Pelkmans *et al.*, 2001), whereas EV1 and CTX (Nichols, 2002) reach these structures in 10–20 min after binding to the cell surface. The difference in kinetics supports the notion

that, in addition to the slow cell surface caveolar pathway described for SV40, EV1 can alternatively enter the caveosomes by a faster pathway.

The final cellular destination of EV1 capsid proteins has remained unclear because of the lack of colocalization with cellular markers used for the rough and smooth ER, the Golgi complex, and lysosomes. SV40 and CTX are directed in a microtubule-dependent, nocodazole-sensitive manner from caveosomes to the ER or the Golgi complex (Pelkmans *et al.*, 2001; Le and Nabi, 2003). Even though tubular structures containing EV1 particles were occasionally observed in live microscopy, the infection was not affected by nocodazole, also indicating that EV1 is not transported to the ER or the Golgi.

BFA, which inhibits several steps of SV40 entry via the caveolar route (Richards *et al.*, 2002), inhibit EV1 infectivity efficiently. However, in the presence of BFA, EV1 was able to reach the intracellular structures that were positive for caveolin-1 and that also accumulated SV40 during coinfection. Thus, it seems likely that the drug may either 1) prevent the uncoating of the virus, 2) stabilize the caveosomal membranes and hence prevent release of the viral genome to the cytoplasm, or 3) prevent the formation of the viral replication complex, as reported for another enterovirus, poliovirus 1 (Maynell *et al.*, 1992).

Before replication in membrane-associated replication complexes in the cytoplasm (Bolten *et al.*, 1998), picornaviruses can release their RNA by several mechanisms. They may form a pore in the plasma membrane or in the membrane of an intracellular vesicle, through which the RNA is then extruded into the cytoplasm (Tosteson and Chow, 1997), or they may uncoat in the acidic environment of endosomes (Schober *et al.*, 1998). For example, poliovirus 1 requires immediate receptor-induced conformational alterations for uncoating (Hogle, 2002). In contrast to many other picornaviruses studied, our sucrose density gradient analysis indicated that EV1 binding to the cell surface is somewhat inefficient in causing disassembly. At the time of uncoating, after 1–2 h of uptake, the viral RNA was largely localized in caveosomes together with EV1 capsid proteins. We have also previously showed that the interaction of EV1 with the α2 integrin I domain does not induce conformational changes of the virus (Xing *et al.*, 2004), and we have isolated an infectious virus from caveosomal vesicles (Marjomäki *et al.*, 2002). These observations suggest that viral capsid proteins and viral RNA are transported to caveosomes before the initiation of viral replication. Because the virus does not move to other cellular locations, such as the Golgi or the ER, the release of the viral genome to the cytoplasm could possibly occur through a pore formed in the caveosomal membrane or by caveosomal rupture. More detailed studies on the exact initiation mechanism of EV1 infection are required to illuminate the role of caveosomes in viral replication cycle.

Our results suggest that EV1 can utilize two distinct pathways of endocytic uptake into host cells. Both are dynamin and lipid raft dependent and can deliver the virus to caveosomes. When compared with SV40, EV1 1) is internalized much faster, 2) does not require actin or microtubules, and, 3) it is not transported to the sER but may uncoat and release its genome into the cytosol at the level of the caveosome. Thus, the overall traffic of EV1 in the caveolar pathway may be significantly different from SV40, a DNA virus that needs to be transported to the nucleus for replication, whereas release of the genome into the cytoplasm is sufficient for a positive-stranded RNA virus to initiate the replication cycle.

ACKNOWLEDGMENTS

We thank J. Bergelson, D. Blaas, A. Dautry-Varsat, S. Fuller, M. McNiven, R. Parton, and M. Steegmaier for the constructs and antibodies used in this study and G.R. Nemerow for insightful comments. C. Krogerus is gratefully acknowledged for help with the FISH technique. M. Vainio is thanked for technical assistance. This work was financially supported by an EMBO short-term fellowship (ASTF 9970) and by grants from the Helsinki Graduate School of Biotechnology and Molecular Biology, the Academy of Finland, the Sigrid Juselius Foundation, the Finnish Cultural Foundation and the Paulo Foundation. L.P. was supported by a TH grant from the Swiss Federal Institute of Technology, and A.H. by a grant from the Swiss National Science Foundation.

REFERENCES

Anderson, H.A., Chen, Y., and Norkin, L.C. (1996). Bound simian virus 40 translocates to caveolin-enriched membrane domains, and its entry is inhibited by drugs that selectively disrupt caveolae. Mol. Biol. Cell *7*, 1825–1834.

Anderson, H.A., Chen, Y., and Norkin, L.C. (1998). MHC class I molecules are enriched in caveolae but do not enter with simian virus 40. J. Gen. Virol. *79*(Pt 6), 1469–1477.

Benlimame, N., Le, P.U., and Nabi, I.R. (1998). Localization of autocrine motility factor receptor to caveolae and clathrin-independent internalization of its ligand to smooth endoplasmic reticulum. Mol. Biol. Cell *9*, 1773–1786.

Benmerah, A., Bayrou, M., Cerf-Bensussan, N., and Dautry-Varsat, A. (1999). Inhibition of clathrin-coated pit assembly by an Eps15 mutant. J. Cell Sci. *112*(Pt 9), 1303–1311.

Bergelson, J.M., St. John, N.F., Kawaguchi, S., Pasqualini, R., Berdichevsky, F., Hemler, M.E., and Finberg, R.W. (1994). The I domain is essential for echovirus 1 interaction with VLA-2. Cell Adhes. Commun. *2*, 455–464.

Bolten, R., Egger, D., Gosert, R., Schaub, G., Landmann, L., and Bienz, K. (1998). Intracellular localization of poliovirus plus- and minus-strand RNA visualized by strand-specific fluorescent in situ hybridization. J. Virol. *72*, 8578–8585.

Cao, H., Garcia, F., and McNiven, M.A. (1998). Differential distribution of dynamin isoforms in mammalian cells. Mol. Biol. Cell *9*, 2595–2609.

Damke, H., Baba, T., Warnock, D.E., and Schmid, S.L. (1994). Induction of mutant dynamin specifically blocks endocytic coated vesicle formation. J. Cell Biol. *127*, 915–934.

DeTulleo, L., and Kirchhausen, T. (1998). The clathrin endocytic pathway in viral infection. EMBO J. *17*, 4585–4593.

Dinter, A., and Berger, E.G. (1998). Golgi-disturbing agents. Histochem. Cell Biol. *109*, 571–590.

Ford, M.G., Pearse, B.M., Higgins, M.K., Vallis, Y., Owen, D.J., Gibson, A., Hopkins, C.R., Evans, P.R., and McMahon, H.T. (2001). Simultaneous binding of PtdIns(4,5)P2 and clathrin by AP180 in the nucleation of clathrin lattices on membranes. Science *291*, 1051–1055.

Grist, N.R., Bell, E.J., and Assaad, F. (1978). Enteroviruses in human disease. Prog. Med. Virol. *24*, 114–157.

Hailstones, D., Sleer, L.S., Parton, R.G., and Stanley, K.K. (1998). Regulation of caveolin and caveolae by cholesterol in MDCK cells. J. Lipid Res. *39*, 369–379.

Henley, J.R., Krueger, E.W., Oswald, B.J., and McNiven, M.A. (1998). Dynamin-mediated internalization of caveolae. J. Cell Biol. *141*, 85–99.

Hogle, J.M. (2002). Poliovirus cell entry: common structural themes in viral cell entry pathways. Annu. Rev. Microbiol. *56*, 677–702.

Huber, M., Brabec, M., Bayer, N., Blaas, D., and Fuchs, R. (2001). Elevated endosomal pH in HeLa cells overexpressing mutant dynamin can affect infection by pH-sensitive viruses. Traffic *2*, 727–736.

Ivaska, J., Reunanen, H., Westermarck, J., Koivisto, L., Kähäri, V.M., and Heino, J. (1999). Integrin alpha2beta1 mediates isoform-specific activation of p38 and upregulation of collagen gene transcription by a mechanism involving the alpha2 cytoplasmic tail. J. Cell Biol. *147*, 401–416.

Joki-Korpela, P., Marjomäki, V., Krogerus, C., Heino, J., and Hyypiä, T. (2001). Entry of human parechovirus 1. J. Virol. *75*, 1958–1967.

Le, P.U., Guay, G., Altschuler, Y., and Nabi, I.R. (2002). Caveolin-1 is a negative regulator of caveolae-mediated endocytosis to the endoplasmic reticulum. J. Biol. Chem. *277*, 3371–3379.

Le, P.U., and Nabi, I.R. (2003). Distinct caveolae-mediated endocytic pathways target the Golgi apparatus and the endoplasmic reticulum. J. Cell Sci. *116*, 1059–1071.

Manders, E.M.M., Verbeej, F.J., and Aten, J.A. (1993). Measurement of co-localization of objects in dual-color confocal images. J. Microsc. *169*, 375–382.

Marjomäki, V. *et al.* (2002). Internalization of echovirus 1 in caveolae. J. Virol. *76*, 1856–1865.

Marjomäki, V.S., Huovila, A.P., Surkka, M.A., Jokinen, I., and Salminen, A. (1990). Lysosomal trafficking in rat cardiac myocytes. J. Histochem. Cytochem. *38*, 1155–1164.

Maynell, L.A., Kirkegaard, K., and Klymkowsky, M.W. (1992). Inhibition of poliovirus RNA synthesis by brefeldin A. J. Virol. *66*, 1985–1994.

Meier, O., Boucke, K., Hammer, S.V., Keller, S., Stidwill, R.P., Hemmi, S., and Greber, U.F. (2002). Adenovirus triggers macropinocytosis and endosomal leakage together with its clathrin-mediated uptake. J. Cell Biol. *158*, 1119–1131.

Mineo, C., Ying, Y.S., Chapline, C., Jaken, S., and Anderson, R.G. (1998). Targeting of protein kinase Calpha to caveolae. J. Cell Biol. *141*, 601–610.

Montesano, R., Roth, J., Robert, A., and Orci, L. (1982). Non-coated membrane invaginations are involved in binding and internalization of cholera and tetanus toxins. Nature *296*, 651–653.

Murata, M., Peränen, J., Schreiner, R., Wieland, F., Kurzchalia, T.V., and Simons, K. (1995). VIP21/caveolin is a cholesterol-binding protein. Proc. Natl. Acad. Sci. USA *92*, 10339–10343.

Nichols, B.J. (2002). A distinct class of endosome mediates clathrin-independent endocytosis to the Golgi complex. Nat. Cell Biol. *4*, 374–378.

Nomura, R., and Fujimoto, T. (1999). Tyrosine-phosphorylated caveolin-1, immunolocalization and molecular characterization. Mol. Biol. Cell *10*, 975–986.

Norkin, L.C., Anderson, H.A., Wolfrom, S.A., and Oppenheim, A. (2002). Caveolar endocytosis of simian virus 40 is followed by brefeldin A-sensitive transport to the endoplasmic reticulum, where the virus disassembles. J. Virol. *76*, 5156–5166.

Ochoa, G.C. *et al.* (2000). A functional link between dynamin and the actin cytoskeleton at podosomes. J. Cell Biol. *150*, 377–389.

Oh, P., McIntosh, D.P., and Schnitzer, J.E. (1998). Dynamin at the neck of caveolae mediates their budding to form transport vesicles by GTP-driven fission from the plasma membrane of endothelium. J. Cell Biol. *141*, 101–114.

Ohman, T., King, S.L., Krithivas, A., Cunningham, J., Dickeson, S.K., Santoro, S.A., and Bergelson, J.M. (2001). Echoviruses 1 and 8 are closely related genetically, and bind to similar determinants within the VLA-2 I domain. Virus Res. *76*, 1–8.

Palade, G. (1953). Fine structure of blood capillaries. J. Appl. Physiol. *24*, 1424–1436.

Parton, R.G., Joggerst, B., and Simons, K. (1994). Regulated internalization of caveolae. J. Cell Biol. *127*, 1199–1215.

Parton, R.G., Way, M., Zorzi, N., and Stang, E. (1997). Caveolin-3 associates with developing T-tubules during muscle differentiation. J. Cell Biol. *136*, 137–154.

Pelkmans, L., and Helenius, A. (2003). Insider information: what viruses tell us about endocytosis. Curr. Opin. Cell Biol. *15*, 414–422.

Pelkmans, L., Kartenbeck, J., and Helenius, A. (2001). Caveolar endocytosis of simian virus 40 reveals a new two-step vesicular-transport pathway to the ER. Nat. Cell Biol. *3*, 473–483.

Pelkmans, L., Puntener, D., and Helenius, A. (2002). Local actin polymerization and dynamin recruitment in SV40-induced internalization of caveolae. Science *296*, 535–539.

Pietiäinen, V., Huttunen, P., and Hyypiä, T. (2000). Effects of echovirus 1 infection on cellular gene expression. Virology *276*, 243–250.

Richards, A.A., Stang, E., Pepperkok, R., and Parton, R.G. (2002). Inhibitors of COP-mediated transport and cholera toxin action inhibit simian virus 40 infection. Mol. Biol. Cell *13*, 1750–1764.

Rothberg, K.G., Heuser, J.E., Donzell, W.C., Ying, Y.S., Glenney, J.R., and Anderson, R.G. (1992). Caveolin, a protein component of caveolae membrane coats. Cell *68*, 673–682.

Roy, S., Luetterforst, R., Harding, A., Apolloni, A., Etheridge, M., Stang, E., Rolls, B., Hancock, J.F., and Parton, R.G. (1999). Dominant-negative caveolin inhibits H-Ras function by disrupting cholesterol-rich plasma membrane domains. Nat. Cell Biol. *1*, 98–105.

Sabharanjak, S., Sharma, P., Parton, R.G., and Mayor, S. (2002). GPI-anchored proteins are delivered to recycling endosomes via a distinct cdc42-regulated, clathrin-independent pinocytic pathway. Dev. Cell *2*, 411–423.

Schober, D., Kronenberger, P., Prchla, E., Blaas, D., and Fuchs, R. (1998). Major and minor receptor group human rhinoviruses penetrate from endosomes by different mechanisms. J. Virol. *72*, 1354–1364.

Shin, J.S., Gao, Z., and Abraham, S.N. (2000). Involvement of cellular caveolae in bacterial entry into mast cells. Science *289*, 785–788.

Simons, K., and Toomre, D. (2000). Lipid rafts and signal transduction. Nat. Rev. Mol. Cell. Biol. *1*, 31–39.

Snyers, L., Zwickl, H., and Blaas, D. (2003). Human rhinovirus type 2 is internalized by clathrin-mediated endocytosis. J. Virol. *77*, 5360–5369.

Steegmaier, M., Yang, B., Yoo, J.S., Huang, B., Shen, M., Yu, S., Luo, Y., and Scheller, R.H. (1998). Three novel proteins of the syntaxin/SNAP-25 family. J. Biol. Chem. *273*, 34171–34179.

Stuart, A.D., Eustace, H.E., McKee, T.A., and Brown, T.D. (2002). A novel cell entry pathway for a DAF-using human enterovirus is dependent on lipid rafts. J. Virol. *76*, 9307–9322.

Sukumaran, S.K., Quon, M.J., and Prasadarao, N.V. (2002). *Escherichia coli* K1 internalization via caveolae requires caveolin-1 and protein kinase Calpha interaction in human brain microvascular endothelial cells. J. Biol. Chem. *277*, 50716–50724.

Thomsen, P., Roepstorff, K., Stahlhut, M., and van Deurs, B. (2002). Caveolae are highly immobile plasma membrane microdomains, which are not involved in constitutive endocytic trafficking. Mol. Biol. Cell *13*, 238–250.

Tosteson, M.T., and Chow, M. (1997). Characterization of the ion channels formed by poliovirus in planar lipid membranes. J. Virol. *71*, 507–511.

Upla, P., Marjomaki, V., Kankaanpaa, P., Ivaska, J., Hyypia, T., Van Der Goot, F.G., and Heino, J. (2004). Clustering induces a lateral redistribution of alpha 2 beta 1 integrin from membrane rafts to caveolae and subsequent protein kinase C-dependent internalization. Mol. Biol. Cell *15*, 625–636.

Xing, L. *et al.* (2004). Structural and functional analysis of integrin alpha2I domain interaction with echovirus 1. J. Biol. Chem. *279*, 11632–11638.